Space Discretization Methods

B. Courbet, C. Benoit, V. Couaillier, F. Haider, M.C. Le Pape, S. Péron

B. Courbet, C. Benoit, V. Couaillier, F. Haider, M.C. Le Pape, S. Péron

(Onera)

E-mail: : bernard.courbet@onera.fr

Space Discretization Methods

Onera codes for CFD and Energetics are mostly based on a finite volume methodology. Within this common framework, a wide variety of space discretization techniques are available depending on the required degree of precision, on the kind of mesh and on the application domain. This paper describes three particular topics which are central to the codes developed at Onera. The first section discusses cell-centered and cell-vertex techniques in the context of structured meshes and their extension to unstructured zones. The second part shows how efficient third order schemes can be implemented on Cartesian and curvilinear overlapping grids. Finally, the third section presents a Muscl-type discretization methodology currently used on general polyhedral meshes, with indications on its generalization to high-order precision.

Introduction

This paper presents some of the space discretization methods used in the codes developed at Onera for Fluid Dynamics and Energetics (see [6] [33] for overall descriptions of ElsA and CEDRE and [34] [37] for examples of applications). All the other numerical and modelization issues will be presented in separate papers; for instance time integration will be found in [28].

Many other projects on innovative methods are underway at Onera and may be a future source of progress for industrial and research codes [3] [25].

Both codes are based on a finite volume methodology [19], with concerns focused on common topics, such as:

- Precision is an essential quality of numerical results. Standard second order interpolation procedures may not be sufficient for applications such as acoustics or Large Eddy Simulations, and several higher order techniques under development or already in application will be described;
- Stability and robustness is an essential requirement for an intensive use on a large number of physical configurations;
- Computational efficiency (memory requirements and execution time) is important as complex simulations are very demanding in terms of computer resources;
- Geometric complexity is increasing in everyday research and industrial applications. Depending on the type of application, structured or non-structured meshes can be used to deal with this issue. Even within the restrictive framework of space discretization, methods cannot be described in detail and only a few important themes have been selected for this presentation.

The remainder of this paper consists in three sections:

- The first one, Finite volume cell centered discretization for MB-structured and hybrid meshes (V. Couaillier, M.C. Le Pape) discusses basic choices for finite volume space discretization on hexahedral meshes including non-structured zones;
- The second section, Third-order scheme in an overset grids framework (C. Benoit, S.Péron) shows how geometric complexity can be taken into account through overlapping structured or Cartesian meshes while maintaining third order precision;
- The last section, Finite volume techniques on polyhedral meshes (B. Courbet, F.Haider) describes the Muscl-type space discretization on general non-structured meshes implemented in CEDRE. These methods can be applied to any kind of polyhedral cells and are thus very well suited to complex geometries. The paper also shows how third-or fourth order interpolation is possible in this framework.

The methods described in the two first sections have been implemented in ElsA, whereas the third part is related to CEDRE.

Finite volume cell centered discretization for mb-stuctured and hybrid meshes

Introduction

This part summarizes some aspects of finite volume space discretization in multi-block structured and hybrid solvers developed at Onera, especially for curvilinear meshes adapted to industrial type applications, that is to say complex mesh topologies. As this presentation is far from exhaustive in terms of the possibilities of a finite volume discretization scheme, we refer the reader to Fletcher [14], Hirsch [20],

Peyret and Taylor [32], for instance, for more detailed presentations of the computational methods for Fluid Dynamics in curvilinear meshes.

Generally speaking, the extension to a multidimensional scheme of 1D numerical schemes is not straightforward. In fact, for a given method defined in 1D, several parameters can vary in 2D and 3D, for example:

- The mesh topology, which is a main point for the numerical method implementation, can be based on different approaches: Mono-domain or multi-domain structured, unstructured, structured/unstructured hybrid. Moreover, adaption techniques may be considered: mesh deformation, mesh motion, local refinement, Automatic Mesh Refinement (AMR).
- The discretisation approach : Finite Differences, Finite Volumes, Finite Elements.

If we restrict the method to finite volume schemes considered in this paper, we still have to specify the unknown localization (numerical field): Cell vertex (control volume = mesh cell + node redistribution), Node centered (control volume = dual mesh cell centered on a mesh node), Cell centered (control volume = mesh cell). The following paragraph is devoted to highlighting some of the choices which were made in elsA. software [7].

Cell centered FV in Multi-block structured meshes

Lax-Wendroff Scheme

Several extensions of the Lax-Wendroff scheme have been proposed in multi-space-dimensions, for the Euler and the Navier-Stokes equations, differing by their non-linear properties and their molecular dependence. For more details concerning these properties, see the complete study done by Lerat [26].

One original formulation of the Lax-Wendroff scheme associated with an efficient multi-grid method has been proposed by Ni for Euler and Navier-Stokes turbomachinery simulation [31], and then used by several authors (see for instance [10] or [15]. This formulation, which is a cell-vertex approach, is very easy to implement but does not preserve the good numerical properties of the original Lax-Wendroff scheme extended on a curvilinear mesh by Lerat [26] (the Ni's scheme is not dissipative in the sense of Kreiss).

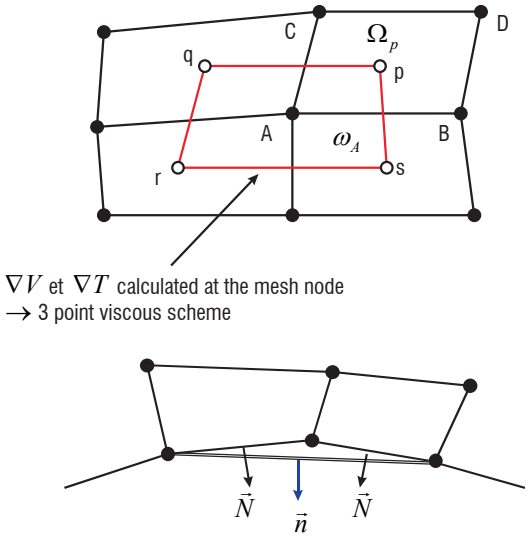

Figure 1 - Lax-Wendroff-Ni scheme

Figure 1 presents the two types of control volumes used in the Lax-Wenfroff-Ni scheme for the space-discretization, the mesh cell control volume and the dual cell control volume, as well as the two types of surface normals used for the treatment of the boundary conditions. The time derivatives are replaced by space derivatives by using the following relation:

$$w_A^{n+1} = w_A^n - \Delta t \vec{\nabla}.(F_C - F_V)_A^n + \frac{\Delta t^2}{2}\vec{\nabla}.(A\vec{\nabla}.(F_C - F_V))_A^n \qquad (1)$$

The gradients appearing in the viscous terms are evaluated at the nodes by using an integral formula based on a dual control volume:

$$\vec{\nabla}\vec{V}_A = \frac{1}{V(\omega_a)}\int_{\partial\omega_a} \vec{V} \otimes \vec{n} ds \qquad (2)$$

Then the first order term is evaluated at the centers of the mesh cells:

$$\vec{\nabla}.(F_C - F_V)_p = \frac{1}{V(\Omega_p)}\int_{\partial\Omega_p} (F_C - F_V) ds \qquad (3)$$

and then distributed at the nodes by using an arithmetic averaging

$$\vec{\nabla}.\varphi_A = \frac{1}{4}\sum_{j=p,q,r,s} \vec{\nabla}.\varphi_j$$ or a volume averaging (Hall approach).

From the first order terms approximated at the cell centers, the second order term can be evaluated directly at the nodes by using a relation analogous to (2), or by using the distribution formulae introduced by Ni for his multi-grid scheme. The artificial dissipation terms are calculated following each mesh direction.

Jameson scheme

This scheme is in fact the most popular scheme used in the CFD community and many 3D research or industrial structured codes developed for complex configurations are based on this approach [21]. Nevertheless, among these codes, two main approaches exist: the node centered approach (for instance [8] [22]) and the cell centered approach (see for instance [5], [40]), with various implementations of the original numerical dissipation adapted to the type of the mesh. The cell vertex approach seems to be more accurate near bodies for the Euler simulations, but this advantage disappears for Navier-Stokes simulations due to the mesh refinement. The main advantage of the cell centered approach is that, in a multi-domain structured approach, there is no problem of multiple point matching (Figure 2-a) or multiple boundary conditions at a given point, and this leads to a robust method for solving complex geometrical configurations. However, in the cell vertex approach, a correct treatment for a point located at a several domain intersection is possible (Figure 2-b), but more difficult to implement in a general approach for structured codes because it depends on the number of domains, as presented in figure 3.

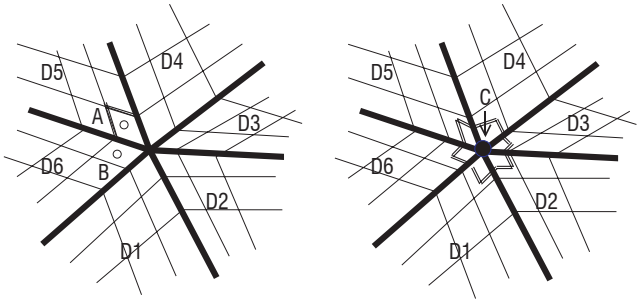

a) Cell centered approach b) Cell vertex approach

Figure 2 - multi-domain interface treatment

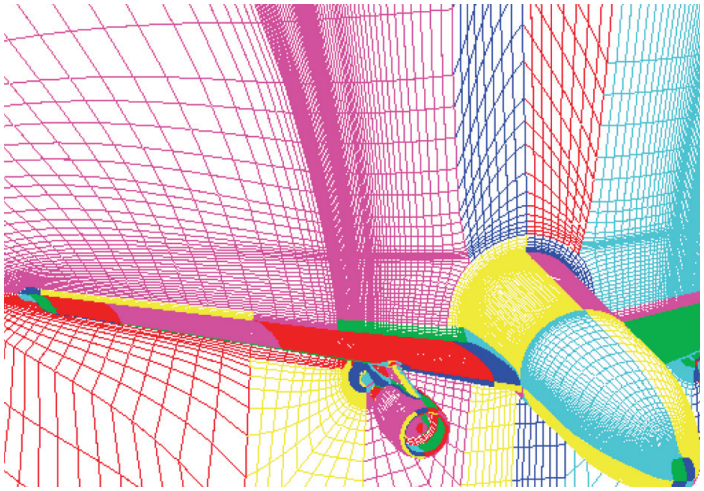

Figure 3 - Wing/Fuselage/Pylon/engine configuration – Multi-block structured mesh

The Jameson scheme is presented below in its cell centered version:

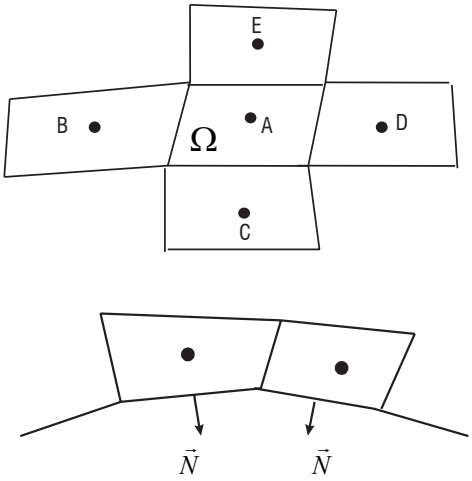

Figure 4 - Cell centered discretization for the Jameson scheme

Figure 4 presents an inner cell control volume used for the space-discretization of the cell centered Jameson scheme, and a boundary cell control volume.

At each step of the Runge-Kutta time-stepping, the solution is updated as follows:

$$w_A^{(p+1)} = w_A^{(0)} - \Delta t \vec{\nabla}.(F_C^{(p)} - F_V^{(0)})_A \qquad (4)$$

The gradient of the velocity is discretized using a mean formula :

$$\vec{\nabla}\vec{V}_A = \frac{1}{V(\Omega_A)} \int_{\partial\Omega_A} \vec{V} \otimes \vec{n} ds \text{ : viscous term calculation} \qquad (5)$$

Then the divergence term can be estimated by using the same type of mean formula:

$$\vec{\nabla}.(F_C - F_V)_A = \frac{1}{V(\Omega_A)} \int_{\partial\Omega_A} (F_C - F_V)\vec{n} ds$$

where a space centered discretization is performed:

$$\int_{\partial\Omega_{AD}} (F_C - F_V)\vec{n} ds = \frac{1}{2}\left[(F_C - F_V)_A + (F_C - F_V)_D\right] \int_{\partial\Omega_{AD}} \vec{n} ds \qquad (6)$$

As for the Lax-Wendroff scheme, the artificial dissipation terms are calculated following each mesh direction.

In the space discretization presented before, the way used for discretizing the viscous term, which is very easy to implement because only one type of control volume is used, corresponds to a five-point scheme. This leads to decoupling odd and even points, this being a drawback from a numerical point of view, because additional artificial dissipation is required even in the viscous region as boundary layers. This can play a significant role when looking at very accurate solutions for basic configurations.

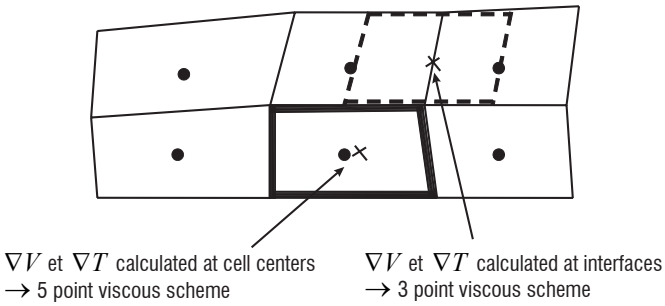

Figure 5 - Viscous term discretization

Then, a three-point scheme (per mesh direction) can be obtained by using staggered cells in each space direction as presented in figure 5, for which the gradients are evaluated at the face centers. In that case, odd and even points are coupled and no artificial dissipation is required in the viscous region, but this approach is more expensive and more difficult to implement in a multi-domain code. Nevertheless, from a practical point of view and for complex configurations in which meshes are not regular, the five-point scheme is widely used.

FV Hybrid solvers on composite meshes

Numerical methods used for the simulation of three-dimensional compressible viscous flows have reached a high level of validity and efficiency and are used as a basic tool for designing turbomachinery and aircraft components. However, most of these methods are based on multi-domain structured grid solvers, which imply a time-consuming mesh generation phase, especially when complex industrial geometries are concerned, and also restrains the application of automatic grid adaptation technologies. On the other hand, the unstructured mesh approach enables the use of automatic mesh generators even on complex geometries, and increases the flexibility for mesh adaptation strategies. A new numerical procedure is developed for the resolution of the three-dimensional Euler and Reynolds-Averaged Navier-Stokes equations. It allows for the implementation in a single global solver of unstructured and hybrid structured-unstructured grids in order to combine as much as possible the efficiency and accuracy of structured solvers and the flexibility and adaptativeness capabilities of unstructured solvers.

At Onera, the first developments on hybrid solvers (as defined above) were carried-out in the years 1994-1998 [23] [24]. The method developed in this work for the solution of the Euler and Reynolds-Averaged Navier-Stokes equations in 3D by means of adaptive unstructured and hybrid grids has clearly demonstrated its value in industrial applications, in which the flexibility of unstructured mesh generation and adaptation is a critical necessity. Satisfactory agreement between ex-

perimental data and computed results validated the numerical method implemented for the resolution of the Euler and Reynolds-Averaged Navier-Stokes equations. An original local mesh enrichment method has been developed and applied on two- and three-dimensional test cases. Convergence acceleration techniques based on agglomeration muti-grid methods was also built up.

Since 2007 this work has been implemented in elsA, and the project elsA-hybrid is now includes new inline development with the end users' requirements for external flow and internal flow simulations (industrial partners, in-house Onera users). In the present part we will briefly describe some aspects of the numerical method implemented for the unstructured meshes as well as the matching techniques between structured and unstructured blocks.

2nd order FV scheme in unstructured meshes

Unstructured solver

The space discretization used at the present time is based on a finite volume decomposition of the computational domain in polygonal control volumes corresponding to the cells of the mesh, leading then to the so-called cell-centered approach. Two different spatial schemes have been implemented:

- A space-centered scheme combined with non linear 2nd order and linear 4th order artificial dissipation terms (Jameson type);
- An upwind method based on the Roe's Flux Difference Splitting scheme and a MUSCL extrapolation of Van Leer, with various limiters.

Both approaches are second order accurate in space on regular meshes, (except near flow discontinuities where a first order accuracy is recovered as for the structured schemes). The treatment of the boundary conditions is based on characteristic relations.

The time integration process uses a multi-step method, either the classical 4-step Runge-Kutta method or the backward Euler method, and is performed in a single time loop including structured and unstructured blocks. Implicit methods are developed, first a LU-SSOR method [28] adapted to unstructured meshes.

Structured / Unstructured block matching technique

The mesh generation flexibility associated with unstructured methods makes it possible in principle to easily ensure point coincidence at the structured block / unstructured block boundaries. In this case the use of a cell-centred scheme in both types of meshes allows for conservative treatment on these block boundaries thanks to the exchange of numerical fluxes through the same interfaces (see Figure 6a). In this case, we use 2nd order FV schemes and the numerical fluxes are computed by means of the values evaluated respectively on the left side and on the right side of the interface and then corresponding either to a structured or to an unstructured reconstruction scheme. This means that the common flux defined at the interface corresponds to a hybrid methodology, the local consistency and the stability of the time-loop process deriving, from a heuristical point of view, from the properties of the separate structured and unstructured schemes.

For various reasons, the use of a node-centered unstructured solver could be of value: number of unknowns, accuracy, etc.; leading to non-conformal matching boundaries (Figure 6b). In that case we must use either interpolation techniques to compute the fluxes on both sides separately [23], or local mesh reconstruction to get common space discretization on the common boundaries [4]. The first solution is not conservative in the principle, but if the cell sizes are close together, the corresponding error is small, whereas the second treatment provides the conservativity property but is more difficult to implement for general curvilinear boundaries in 3D meshes.

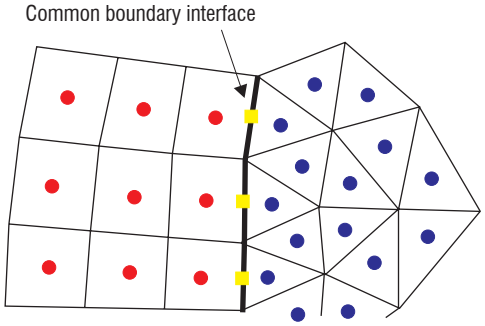

a)

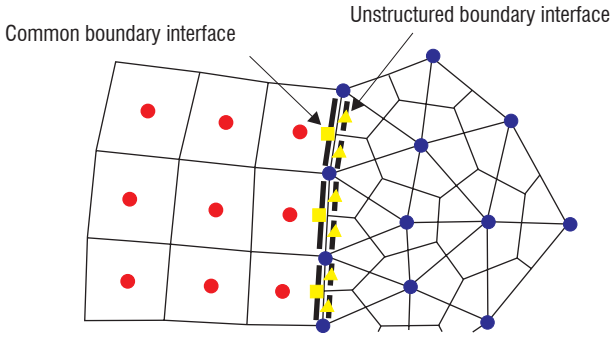

b)

Figure 6 - Structured / unstructured block matching – Cell vertex versus cell centered

Mesh adaptation

Automatic mesh adaptation tends to correct the numerical error inherent to an initial improper grid node distribution. Isotropic as well as anisotropic mesh refinements have been studied and implemented at Onera.

A method for the automatic adaptation of unstructured grids has been proposed in [24]. The basis of this method comes from a local anisotropic mesh enrichment idea. Most of the refinement procedures applied on unstructured grids are based on an isotropic division of cells. On the contrary, the present method relies on an anisotropic division of cells over the edges. An original error estimator, which is obtained from an evaluation of the interpolation error on the edges of the mesh, takes into account the mixed discretization of the solution in a first order accurate part near discontinuities, and a second order accurate part elsewhere. This error estimator is applied to determine which cells of the mesh have to be divided. After each step of enrichment, the distorted mesh is optimized by Laplacian-like smoothing and edge swapping. Applications of the adaptation procedure coupled with the numerical method have been used on several test cases (airfoil, wing, isolated rotor). There are plans to couple with the elsA software in the near future.

The first computations with unstructured isotropic mesh refinements were recently performed with elsA. Mach number gradient computation across interfaces determines which cells must be divided. Applications of the adaptation procedure coupled with the numerical method are fulfilled on the NACA0012 airfoil and on the ONERA M6

wing. The value of this adaptation procedure is clearly seen in the presented result (Figure 7) with the excellent capture of the flow features after four cycles of adaptations/CFD computations.

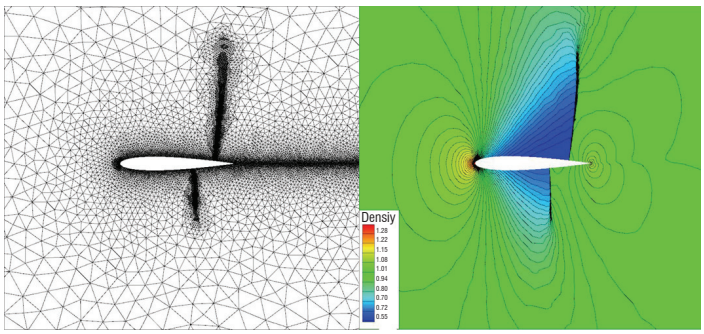

Figure 7 - NACA0012 airfoil – Euler transonic computation – unstructured mesh refinement

Third-order scheme in an overset grids framework

Introduction

In this part, the computational domain is discretized by a set of curvilinear structured grids around bodies completed by a set of regular Cartesian grids.

There are various reasons to justifying the choice of this grid topology. First, on structured grids (that is i,j,k-ordered grids), the numerical scheme is generally more computationally efficient than on unstructured grids (that is grids made of tetrahedrons, hexahedrons, etc. with no particular order). Besides, various studies have proven that a numerical scheme on Cartesian grids is even more efficient and accurate. As a matter of fact, on regular Cartesian grids, numerical scheme formulae are simplified and no metrics storage is required. Another advantage of Cartesian grids is the simplicity of the formulation of high-order schemes.

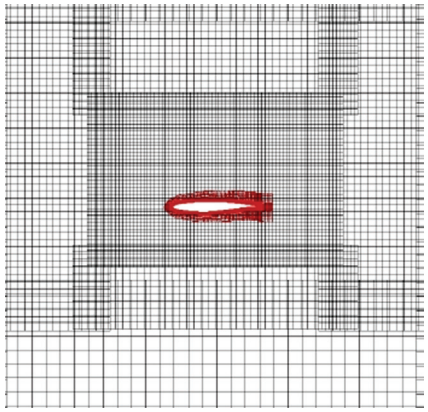

Figure 8 - Example of curvilinear-Cartesian topology around a 2D airfoil

An example of the kind of mesh topology studied here is given in figure 8. The shortly extended meshes around the airfoil are structured and the remaining part of the domain is meshed with regular structured Cartesian grids. All of the grids are overset, which means that an overlap between all grids exists. Fluid variables are transferred between all grids using interpolations in those overlap regions. The transfer technique used here is called Chimera and was first introduced by Steger et al. [38]. The set of Cartesian grids is automatically generated, given the set of curvilinear grids around the bodies and it can be also adapted to the solution during the computation. The method can be also applied with unstructured grids around the bodies (see [41]).

This kind of mesh topology has been first introduced by Meakin [29] and also developped by Benoit and Jeanfaivre [2] with applications to helicopter rotor flows in hover.

This part of the paper presents the adaptation of a third-order numerical scheme to this kind of mesh topology. More details can be found in [19]. We first present the third-order scheme on curvilinear grids, then its formulation on Cartesian grids. Finally, we present the adaptation of this scheme to overlap boundaries together with third-order interpolations.

Third-order finite volume scheme on curvilinear meshes

On curvilinear grids, a third-order space accurate scheme is used. This scheme is based on the work of Cinnella, Lerat and Rezgui [35, 9] in a finite-volume formulation. For the sake of simplicity, this scheme is presented in 2D and for the Euler equations. Let p,η,u,v,E and H denote the pressure, density, Cartesian velocity components, total energy and total enthalpy. For a perfect gas:

$$p=(\gamma-1)\rho\left(E-\frac{u^2+v^2}{2}\right)$$

where γ is the ratio of specific heats. The Euler equations for two dimensional inviscid flow can be written in integral form:

$$\frac{d}{dt}\int_{\Omega} w\,d\Omega+\int_{\partial\Omega}F(w).n\,d\Gamma=0 \qquad (7)$$

where:

$$w=\begin{pmatrix}\rho\\ \rho u\\ \rho v\\ \rho E\end{pmatrix},\quad f(w)=\begin{pmatrix}\rho u\\ \rho u^2+p\\ \rho uv\\ \rho uH\end{pmatrix},\quad g(w)=\begin{pmatrix}\rho v\\ \rho uv\\ \rho v^2+p\\ \rho uH\end{pmatrix}$$

and Ω is a bounded domain with boundary $\partial\Omega, n$, is the unit outward normal to $\partial\Omega$, and $F(w)=\left[f(w),g(w)\right]$ is the flux density. We define a structured mesh composed of quadrangular cells $\Omega_{j,k}$ (Figure 9) and denote the cell centers by $C_{j,k}$ and the cell edges by $\Gamma_{j+\frac{1}{2},k}$, or $\Gamma_{j,k+\frac{1}{2}}$:

$$\partial\Omega_{j,k}=\{\Gamma_{j+\frac{1}{2},k},\Gamma_{j,k+\frac{1}{2}},\Gamma_{j-\frac{1}{2},k},\Gamma_{j,k-\frac{1}{2}}\}$$

Applied to the cell $\Omega_{j,k}$ the conservation laws (7) become:

$$\frac{d}{dt}\int_{\Omega_{j,k}} w\,d\Omega+\sum_{\Gamma\in\partial\Omega_{j,k}}\int_{\Gamma}F(w).n\,d\Gamma=0$$

The numerical flux density $F_{j+\frac{1}{2},k}$ through the edge $\Gamma_{j+\frac{1}{2},k}$ of the cell $\Omega_{j,k}$, is an approximation to:

$$\frac{1}{|\Gamma_{j+\frac{1}{2},k}|}\int_{\Gamma_{j+\frac{1}{2},k}}F(w).n\,d\Gamma$$

To define a local reference frame on the edge $\Gamma_{j+\frac{1}{2},k}$, let ξ be an axis passing through the adjoining cell center, oriented from $C_{j,k}$ to $C_{j+1,k}$ and let η be an axis on $\Gamma_{j+\frac{1}{2},k}$. Let E be the intersection point of the η and ξ axis.

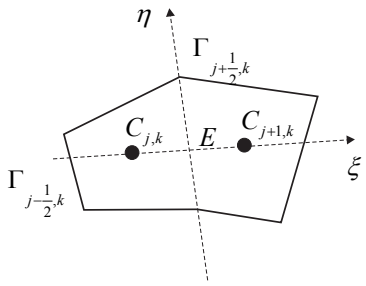

Figure 9 - Definition of the local frame of reference

Performing a Taylor expansion in the η-direction, a third-order approximation of the exact flux is:

$$\frac{1}{|\Gamma_{j+\frac{1}{2},k}|}\int_{\Gamma_{j+\frac{1}{2},k}} F(w).n\, d\Gamma = (\phi + \beta_1\phi_\eta + \beta_2\phi_{\eta\eta})_{|E} + O(h^3) \qquad (8)$$

With $F = F.n$ and:

$$\beta_1 = \frac{\int_\Gamma (\eta - \eta_{|E})\, d\eta}{|\Gamma_{j+\frac{1}{2},k}|} = O(h)$$

$$\beta_2 = \frac{\int_\Gamma (\eta - \eta_{|E})^2\, d\eta}{2\,|\Gamma_{j+\frac{1}{2},k}|} = O(h^2)$$

where η_E is the coordinate of E on the η-axis ($\eta_E = 0$) and

$$b = \left|C_{j,k}C_{j+1,k}\right|$$

To complete the discretization of (8), we must provide third, second and first-order approximations for ϕ_E, ϕ_{η_E} and $\phi_{\eta\eta_E}$ respectively. This is done in a centered way by using weighted average and difference operators taking into account the locations of E and of the surrounding cell centers. A Third-order approximation of ϕ_E is obtained by cancelling the error term introduced by the weighted average which discretizes ϕ_E to second-order accuracy. Numerical flux is third-order accurate [35] on moderately deformed meshes and at least second-order accurate on highly-distorded meshes. If the grid deformations were neglected, the above weighted numerical flux would be reduced to:

$$F_{j+\frac{1}{2},k} = \left(\mu_1\phi - \frac{1}{8}\delta_1^2\mu_1\phi + \frac{1}{24}\delta_2^2\mu_1\phi\right)_{j+\frac{1}{2},k}$$

where δ_1, δ_2, μ_1 and μ_2 denote the following discrete operators:

$$(\delta_1 u)_{j+\frac{1}{2},k} = u_{j+1,k} - u_{j,k}, \qquad (\delta_2 u)_{j,k+\frac{1}{2}} = u_{j,k+1} - u_{j,k}$$

$$(\mu_1 u)_{j+\frac{1}{2},k} = \frac{1}{2}(u_{j+1,k} + u_{j,k}), \qquad (\mu_2 u)_{j,k+\frac{1}{2}} = \frac{1}{2}(u_{j,k+1} + u_{j,k})$$

Formulation of the scheme on a regular Cartesian mesh

Let us express the complete scheme on a regular Cartesian grid, since this type of grid is our main concern in our mesh topology. With $\phi = f$ on $\Gamma_{j+\frac{1}{2},k}$ and $\phi = g$ on $\Gamma_{j,k+\frac{1}{2}}$, the scheme reads:

$$F_{j+\frac{1}{2},k} = \left[(I - \frac{1}{8}\delta_1^2 + \frac{1}{24}\delta_2^2)\mu_1 f\right]_{j+\frac{1}{2},k}$$

$$F_{j,k+\frac{1}{2}} = \left[(I - \frac{1}{8}\delta_2^2 + \frac{1}{24}\delta_1^2)\mu_2 g\right]_{j,k+\frac{1}{2}}$$

The finite volume scheme can be rewritten in the very simple form:

$$\left[w_t + \frac{\delta_1}{\delta x}(I - \frac{1}{6}\delta_1^2)\mu_1 f + \frac{\delta_2}{\delta y}(I - \frac{1}{6}\delta_2^2)\mu_2 g\right]_{j,k} = 0 \qquad (9)$$

This Cartesian scheme is purely directional, i.e it involves points only in the x and y directions passing through the cell center $C_{j,k}$. This formulation of the third-order of the numerical scheme on regular Cartesian grids, which can be seen as a finite difference formulation, is strictly equivalent to the finite volume approach. The expression (9) is much simpler than the general finite volume formula and will be implemented this way on the Cartesian grids of the mesh adaptation method for efficiency reasons.

Numerical dissipation

Centered schemes are non dissipative and are therefore subject to numerical instabilities due to the growth of high-frequency modes. Consequently, the Jameson artificial dissipation [21] is incorporated in previous formulations.

For instance for the Cartesian scheme, this leads to modification of the numerical fluxes in the j direction (with similar modification in the k direction) as follows:

$$F_{j+\frac{1}{2},k} = (F - D)_{j+\frac{1}{2},k}$$

with the dissipation:

$$(D)_{j+\frac{1}{2},k} = \rho(\bar{A}_{j+\frac{1}{2},k})\,(\epsilon_2\delta_1 w - \epsilon_4\delta_1^3 w)_{j+\frac{1}{2},k}$$

where $A_{j+\frac{1}{2},k}$ is an average of the Jacobian matrix $A = df/dw, \rho(A)$ denotes the spectral radius of matrix A and:

$$\epsilon_{2|j+\frac{1}{2},k} = k_2 \max(\nu_{j,k}, \nu_{j+1,k}), \quad \epsilon_{4|j+\frac{1}{2},k} = \max(0, k_4 - \epsilon_{2|j+\frac{1}{2},k})$$

$$\nu_{j,k} = \frac{|\,p_{j+1,k} - 2p_{j,k} + p_{j-1,k}\,|}{|\,p_{j+1,k} + 2p_{j,k} + p_{j-1,k}\,|}$$

where p is the static pressure and k_2, k_4 are constant parameters. In a region where w is smooth, $k_2 = O(h^2)$ and $k_4 = O(1)$, so that the dissipative terms are $O(h^3)$ and the whole scheme remains third-order accurate.

High-order mesh adaptation method

As previously said, the mesh adaptation method of Meakin is based on the Chimera technique. For high-order numerical schemes, it has been demonstrated that linear interpolation is not sufficient to maintain the overall global accuracy of an overset-grid technique at the same order as the interior numerical scheme. The third-order interpolation procedure used here is based on directional Lagrange polynomials. The numerical solution on Grid A at point x is interpolated from points x_0, x_1 and x_2 located on Grid B (Figure 9), the formulae used are:

$$w(x)=\sum_{j=0}^{n} w_j l_j(x), \quad l_j(x)=\frac{\Pi_{k=0,k\neq j}^{n}(x-x_k)}{\Pi_{k=0,k\neq j}^{n}(x_j-x_k)}$$

In order to be more accurate, the third point on Grid B x_0 is chosen such as:

$$\begin{cases} x_0 = x_1 - \delta x \quad if \mid x - x_1 \mid < \dfrac{\delta x}{2} \\ x_0 = x_2 + \delta x \; otherwise \end{cases}$$

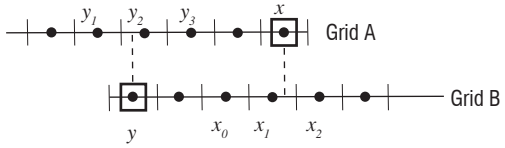

Figure 10 – Interpolated points for high-order Chimera transfers

Modification of schemes near overlap boundaries

In the overlap region, the number of grid points has to be sufficient to ensure a proper communication between the grids. In particular, an interpolated point must be computed from interior points. If a valid interpolation cell cannot be found, the interpolated point is called an orphan point. In our technique, in order to diminish the occurrence of orphan points, only one layer of interpolated cells is used. Nevertheless, the third-order scheme is a five-point stencil scheme and it must therefore be reformulated near interpolated points in order to preserve the global order of accuracy.

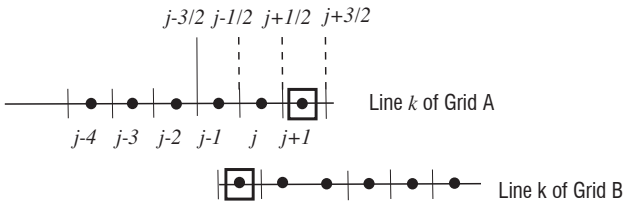

Figure 11 – Minimum overlap with one layer of interpolated cells

In figure 11, the values on the last cell face $(j+3,k)$ of Grid A are always interpolable 2 by Lagrange interpolation, otherwise Grid B would be too small and thus useless. A specific treatment based on upwind formulae is performed for the calculation of physical flux and the artificial viscosity flux at the face $(j+1/2,k)$. It uses the interpolated value 2 $f_{j+\frac{3}{2},k}$:

$$F_{j+\frac{1}{2},k} = -\frac{1}{84}f_{j-2,k} - \frac{1}{60}f_{j-1,k} + \frac{5}{12}f_{j,k} + \frac{11}{12}f_{j+1,k} - \frac{32}{105}f_{j+\frac{3}{2},k}$$

$$D_{j+\frac{1}{2},k} = \rho(\bar{A})_{j+\frac{1}{2},k}\left(\varepsilon_2(w_{j+1,k}-w_{j,k}) - \varepsilon_4\left(\frac{1}{7}w_{j-2,k} - \frac{9}{5}w_{j-1,k} + 5w_{j,k} - 7w_{j+1,k} + \frac{128}{35}w_{j+\frac{3}{2},k}\right)\right)$$

with:

$$v_{j+1,k} = \frac{\left|2p_{j,k} + \frac{16}{5}p_{j+\frac{3}{2},k} - \frac{1}{5}p_{j-1,k} - 5p_{j+1,k}\right|}{\left|2p_{j,k} + \frac{16}{5}p_{j+\frac{3}{2},k} + \frac{1}{5}p_{j-1,k} + 5p_{j+1,k}\right|}$$

These formulae allow to preserve the global third-order of accuracy of the overset grids method.

Application

This methodology was validated in [36] and the practical third-order demonstrated. We present here a simulation of a helicopter isolated blade in forward flight. The tip Mach number is M_{tip} = 0.646, the blade advance ratio is μ = 0.4. In figure 12, the blade mesh together with the set of adapted Cartesian grids is presented for an azimuth of 440 degrees. The total number of points in the mesh is 19 million points. The Q-criterion exhibiting the vortical wake of the blade shows that this wake is well-captured by the adapted mesh.

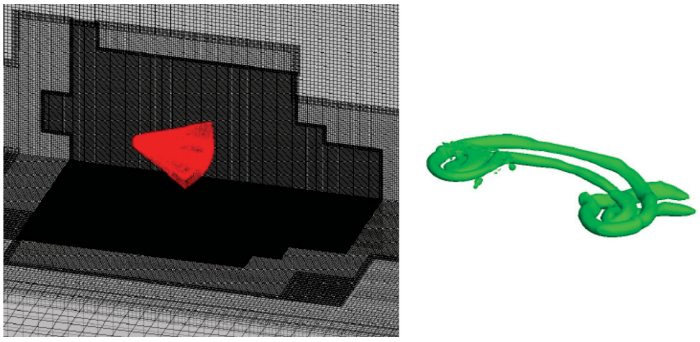

Figure 12 - Mesh and Q-criterion for an isolated blade in forward flight

Finite volumes on polyhedral meshes

Context and motivation

The methods described in this section were originally developed within the CEDRE software [33] for application domains focused on energetics and propulsion, which are often characterized by very complex geometries [37]. With the need to take more and more technological details into account, it quickly became obvious that the setting up of structured hexahedral mesh calculations was often too much time consuming.

On the other hand, many types of automatic mesh generation software were gradually becoming available. Tetrahedral meshers were the first to appear, but current software often mixes several types of elements, for instance tetrahedra, prisms, pyramids and hexahedra. Other kinds of elements are also becoming available in some meshers : hexahedra trimmed by boundaries, hexahedra with refinement, polyhedral mesh obtained as the dual of a tetrahedral original mesh etc.

Furthermore, the mesh can be subjected to a topological alteration in the course of calculation. Adaptive mesh refinement is a well-known example, but another interesting situation is shown on figure 13. In this example, the moving mesh fitted to a rotating solid (green) partly overlaps the Cartesian grid of a the fluid container (blue). The effective mesh used for this ALE calculation is made of the overlapping mesh and the visible part of the Cartesian grid, which is trimmed in a very general way into various polygonal (polyhedral in 3D) shapes. The methods used in this calculation were originally developed in the FLUSEPA software of ASTRIUM and have been subsequently applied to CEDRE.

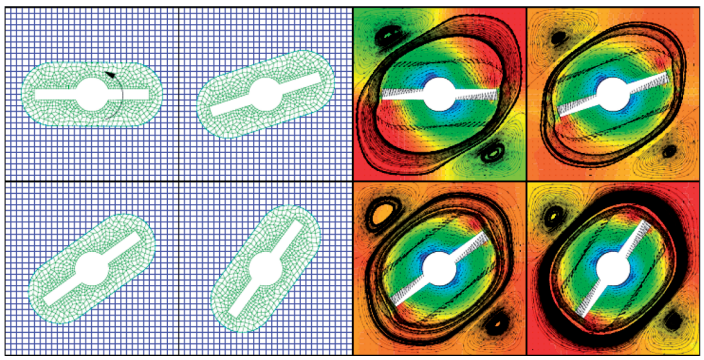

Figure 13 - Conservative overlapping : example of mesh, pressure field and streamlines

These examples show that a general polyhedral mesh of the physical domain is very desirable in dealing with complex flow situations.

The geometric and kinematic model

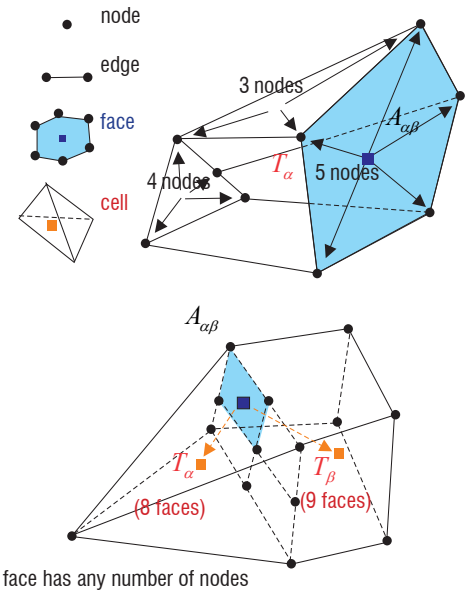

- every face has any number of nodes

- a general polyhedral cell has any number of faces, but one face connects 2 cells

Figure 14 - Polyhedral finite volume cells and faces

The following conditions define a general polyhedral mesh (figure 13):

• Every cell face $A_{\alpha\beta}$ is a triangulation lying on a generally non-planar polygonal contour with any number of vertices. The common point $K_{\alpha\beta}$ of the triangulation can be defined in several ways; one natural choice is to identify $K_{\alpha\beta}$ with the gravity center of the triangulated face.

• Every cell T_α is bounded by any number of faces $A_{\alpha\beta}$. Conversely, an internal face $A_{\alpha\beta}$ always connects two cells T_α and T_β exactly.

If the positions $x_s(t)$ of vertices are known, every cell T_α is completely defined. One can then calculate for instance the surface vector $\boldsymbol{N}_{\alpha\beta}$, area $S_{\alpha\beta}$ and gravity center $x_{\alpha\beta}$ of $A_{\alpha\beta}$,

$$\boldsymbol{N}_{\alpha\beta} \triangleq \int_{A_{\alpha\beta}} \boldsymbol{n}\, dA,\ \boldsymbol{n}_{\alpha\beta} \triangleq \frac{\boldsymbol{N}_{\alpha\beta}}{|\boldsymbol{N}_{\alpha\beta}|},\ S_{\alpha\beta} \triangleq \int_{A_{\alpha\beta}} dA,\ x_{\alpha\beta} \triangleq \frac{1}{S_{\alpha\beta}} \int_{A_{\alpha\beta}} \boldsymbol{x} dA \quad (10)$$

and the volume V_α and gravity center x_α of T_α:

$$V_\alpha \triangleq \int_{T_\alpha} dV \quad , \quad x_\alpha \triangleq \frac{1}{V_\alpha} \int_{T_\alpha} \boldsymbol{x}\, dV \quad (11)$$

The gravity centers of faces and cells are convenient Gauss points allowing exact quadrature for linear functions:

$$\text{If } w(x) \text{ is linear, } \int_{T_\alpha} w(x)\, dV = V_\alpha w(x_\alpha)$$
$$\text{and } \int_{A_{\alpha\beta}} w(x)\, dA = S_{\alpha\beta} w(x_{\alpha\beta}) \quad (12)$$

Figure 15 defines additional notations for the interface $A_{\alpha\beta}$ between two cells T_α and T_β:

$$\boldsymbol{h}_{\alpha\beta} \triangleq x_\beta - x_\alpha\ ,\ a_{\alpha\beta} \triangleq x_{\alpha\beta} - x_\alpha\ ,\ \boldsymbol{b}_{\alpha\beta} \triangleq (a_{\alpha\beta} \cdot \frac{\boldsymbol{h}_{\alpha\beta}}{|\boldsymbol{h}_{\alpha\beta}|}) \frac{\boldsymbol{h}_{\alpha\beta}}{|\boldsymbol{h}_{\alpha\beta}|} \quad (13)$$

The first neighborhood ν_α^1 of T_α is defined as the set of all cells T_β sharing a face $A_{\alpha\beta}$ with T_α, plus T_α itself (figure 15). More generally, the second neigborhood ν_α^2 is made of ν_α^1 plus all the first neighbors of cells inside ν_α^1 etc. The first neighborhood ν_α^1 is convenient for algorithm description, but the reciprocal neighborhood $W_{\alpha\beta}^1$ of face $A_{\alpha\beta}$, which is made of T_α and T_β is equivalent and often more adapted to implementation. Other kinds of neighborhoods (for instance through vertices or edges) could be used, but it was de-

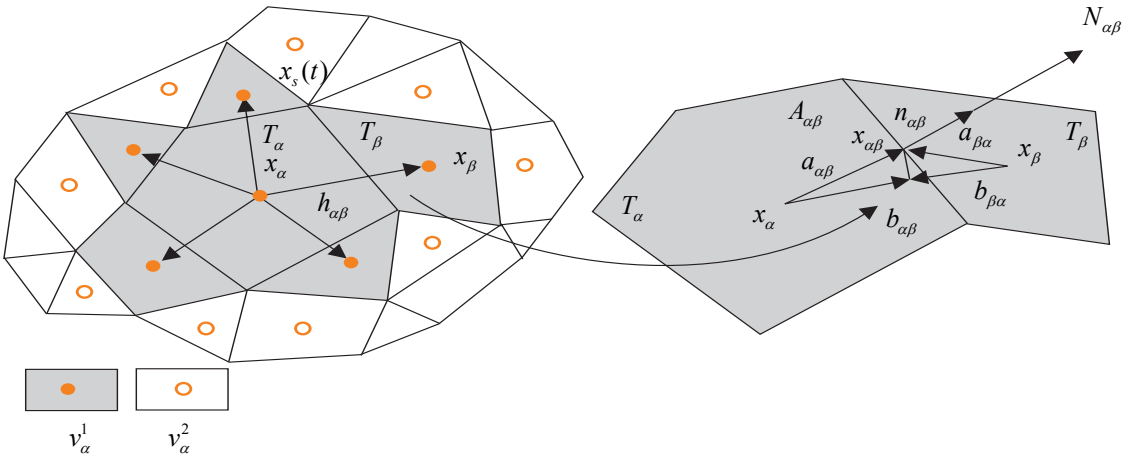

Figure 15 - Geometry of cells and faces and neighborhoods (two-dimensional sketch)

cided for simplicity to base all algorithms only on v_α^1 and its iterates $v_\alpha^2 \ldots v_\alpha^l \ldots$.

This definition of geometry is generally time-dependant. If the movement of every vertex is known, all the above properties of cells and faces are known functions of time.

Governing equations and state variables

In this paper, we consider a continuum characterized by a set of n_q conserved quantities per unit volume depending on space and time $q = q(x,t)$. Alternatively, the local state can also be represented by a system of intensive variables $u = u(x,t)$ which is more convenient in some contexts. Both descriptions are equivalent, i.e. we can define a one-to-one mapping between u and q ,

$$q = Q(u) \quad \text{or} \quad u = U(q) \tag{14}$$

In the special case of a compressible fluid flow with fixed composition, q includes mass, momentum and total energy per unit volume ($n_q = 5$ scalar variables). In the absence of phase transition, a convenient set of intensive variables is made up of pressure, temperature and macroscopic velocity:

$$q = \begin{bmatrix} \rho \\ \rho \mathbf{v} \\ \rho e_t \end{bmatrix}, \quad u = \begin{bmatrix} p \\ T \\ v \end{bmatrix} \tag{15}$$

This particular set of q and u variables is only given as an elementary example, since fluid dynamics and energetics include many other models [13]. For instance, the above definition of u does not hold for flows with phase transition. In Reynolds Averaged turbulent flows, additional quantities describe turbulence [1], whereas the mixture composition introduces further degrees of freedom in aerothermochemistry [13] [12] etc. Completely different systems are also needed, for instance for conduction in solids, particles in the Eulerian approach or fully multiphase flow [33] [30]. Wherever possible, this paper avoids modelization details and concentrates on generic equations and methods for Eulerian solvers, with Lagrangian methods for particles being described in [30].

The keystone of the Eulerian physical models considered in the sequel is a set of balance equations for $q(x,t)$. The most general form of these equations expresses conservation on any moving and possibly deformable control volume $V(t)$ bounded by a surface $A(t)$ with velocity $v_A(x,t)$ (figure 16 a):

$$\forall V(t), \frac{d}{dt}\int_v q dV = -\int_A (q(\mathbf{v}-\mathbf{v}_A)+\boldsymbol{f}+\varphi)\cdot \mathbf{n}\, dA + \int_v s dV \tag{16}$$

Equation (16) states that the quantity of q inside $V(t)$, which is a function of time only, varies under the influence of non dissipative fluxes (flux density $q(v-v_A)+\boldsymbol{f}$, where the first term represents advection), dissipative fluxes (flux density φ) and sources per unit volume. This system of conservation laws must be completed by a thermodynamic model for the continuum [13], phenomenological relationships to express the dissipative fluxes φ and models for sources s , which will be supposed to be of the form

$$\boldsymbol{f} = \boldsymbol{f}(u), \varphi = \varphi(u, \nabla u) \text{ with } \varphi(u,0) = 0, s = s(u, \nabla u, \cdots) \tag{17}$$

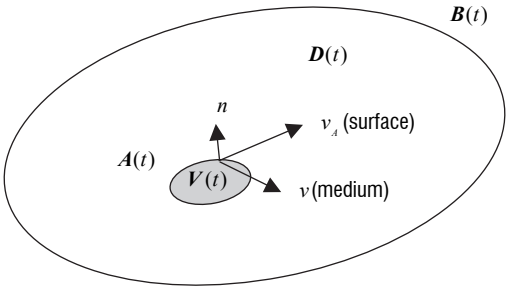

a) Physical domain and boundary control volume $V(t)$

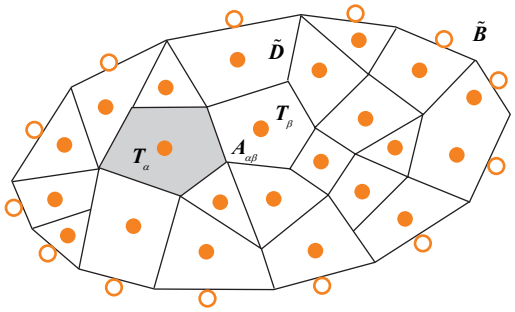

b) Discrete approximation of domain and boundary cells and locations for discrete variables

Figure 16 - Notations for space discretization

Where the field of state variables is sufficiently regular, the integral form (16) is equivalent to a system of partial differential equations

$$\partial_t q = -\nabla\cdot(qv + \boldsymbol{f} + \varphi) + s \tag{18}$$

Conservation equations (16) or (18), (17) must be completed by a proper set of boundary conditions along the limits $x_B(t)$ of the region $D(t)$ of interest and by an initial condition.

If $s = 0$, $q(x,t) = constant$ is a solution of (18). It is of course also a solution of the integral form (16) because

$$\forall V(t), \quad \frac{d}{dt}\int_v dV = \int_A \boldsymbol{v}_A \cdot \mathbf{n}\, dA \tag{19}$$

is a kinematic identity which states that the rate of variation of the volume of $V(t)$ is exactly equal to the volume swept by the surface $A(t)$ per unit time.

A family of Finite Volume methods on general polyhedra

To derive space discretization, one common approach in CFD and connected domains is the finite volume method. In fact, this term does not really describe a method but rather a point of view on space discretization which can lead to a large number of distinct algorithms. The starting point is the balance equation (16) written on a control volume (or cell) defined by T_α . Let us define the volume $V_\alpha(t)$ of T_α

$$V_\alpha(t) \triangleq \int_{T_\alpha} dV \tag{20}$$

and the mean values $q_\alpha(t)$ of conserved quantities on T_α

$$q_\alpha(t) \triangleq \frac{1}{V_\alpha}\int_{T_\alpha} q(\mathbf{x},t) dV \tag{21}$$

With these notations, the balance equation (16) reads

$$\frac{d}{dt}(V_\alpha q_\alpha) = -\sum_{\beta\in v_\alpha^1}\int_{A_{\alpha\beta}} (q(\mathbf{v}-\mathbf{v}_A)+\boldsymbol{f}+\varphi)\cdot\mathbf{n}\, dA + \int_{T_\alpha} s dV \tag{22}$$

where normal flux densities are integrated on all the faces $A_{\alpha\beta}$ of the cell. The mean value $q_\alpha(t)$ is an obvious candidate as the space-discrete degree of freedom associated with T_α, but it is of course equivalent to the use of the set of natural variables $u_\alpha(t) \triangleq U(q_\alpha(t))$ for this purpose.

An important property of the finite volume approach is that it automatically leads to exactly conservative space discretizations: if we sum equations (22) for any cluster $\{T_\alpha\}$ of neighboring cells, the fluxes along internal interfaces cancel and the variation rate of conserved quantities inside the cluster is only due to the integral of fluxes along the limits of $\{T_\alpha\}$ and the volume integral of sources inside $\{T_\alpha\}$. Conservativity is a very desirable property in engineering analysis as it allows a non-ambiguous evaluation of mass, momentum and energy transfers independently of the mesh size.

Up to this point, no approximation has been made and (22) can be considered as exact. The next step will be to derive approximations for fluxes and sources at the right-hand side of (22) as functions of the space-discrete degrees of freedom in a certain neighborhood of face $A_{\alpha\beta}$. The family of finite volume methods implemented in CEDRE can be viewed as an extension of MUSCL schemes to general polyhedral meshes, which were initially defined for structured grids [40]:

- For each cell T_α and fixed t, we define a polynomial reconstruction $w_{q,\alpha}(x)$ (or $w_{u,\alpha}(x)$) which approximates the field of the state variables on T_α (for simplicity, t will be omitted in the statement of w_q and w_u). The reconstruction is designed to be $k-$exact, i.e. exact if each component of the original function is locally a polynomial of degree k. The $l-th$ order derivatives $l=1\cdots k$ defining the polynomial are evaluated algebraically from the state variables on a neighborhood of T_α, for example with the help of a least-squares technique.
- This reconstruction allows the evaluation of state variables at any point of $A_{\alpha\beta}$ with precision $O(h^{k+1})$ (where h is the order of magnitude of $|h_{\alpha\beta}|$) and the reconstruction from cell T_β gives rise to a second evaluation with the same precision. A non-linear limitation formula eliminates possible local extrema in these evaluations. First order derivatives along $A_{\alpha\beta}$ can also be evaluated with the help of both reconstructions.
- The surface and volume integrals at the right-hand side of (22) can be evaluated through Gauss quadrature, with enough quadrature points to meet the precision of the reconstruction.
- Finally, numerical flux formulas adapted to physics must be applied at every Gauss point. This stage is purely local and involves no interpolation.

The precision of the space discretization depends only on interpolation (first and second item above) and quadrature (third item) which are independent of physics, whereas stability also depends on the physics involved in fluxes and sources and their numerical approximations (fourth item).

In (22), all geometric quantities are generally time-dependent due to mesh movement and deformation : this formulation is usually known as ALE (for Arbitrary Lagrangian Eulerian). Volume conservation (19) for T_α reads

$$\frac{dV_\alpha}{dt} = \sum_{\beta\in v_\alpha^1} \int_{A_{\alpha\beta}} v_A \cdot \mathbf{n}\, dA \tag{23}$$

If the motion law of every vertex is known, v_A can be calculated at every point along $A_{\alpha\beta}$, as well as the integrals on the right-hand side of (23). If we set

$$v_{An,\alpha\beta} \triangleq \frac{1}{|\mathbf{N}_{\alpha\beta}|} \int_{A_{\alpha\beta}} v_A \cdot \mathbf{n}\, dA \tag{24}$$

volume conservation simply reads

$$\frac{dV_\alpha}{dt} = \sum_{\beta\in v_\alpha^1} v_{An,\alpha\beta} |\mathbf{N}_{\alpha\beta}| \tag{25}$$

We stress that (25) need not be added as a supplementary ALE equation since it is an automatic consequence of a correct evaluation of time-dependent volume and face velocity. It can be checked that under the preceding general hypotheses for interpolation, constant states $q_\alpha(t) = q^0 = constant$ are automatically solutions of the semi-discrete conservation equations (22) for any mesh movement and deformation.

Methods with piecewise linear reconstruction ($k=1$)

Reconstruction on T_α

The local reconstruction $w_{q,\alpha}(x)$ for $q(x,t)$ is chosen to be linear on T_α :

$$w_{q,\alpha}(x) = q_\alpha + \boldsymbol{\sigma}_{q,\alpha} \cdot (x - x_\alpha) \tag{26}$$

where $\boldsymbol{\sigma}_{q,\alpha}$ is a consistent approximation of the gradient at the center of gravity of T_α

$$\boldsymbol{\sigma}_{q,\alpha} = (\nabla q)_\alpha + O(h). \tag{27}$$

As stated before (12), the mean value of the linear reconstruction is equal to its value at the gravity center x_α :

$$\frac{1}{V_\alpha} \int_{T_\alpha} w_{q,\alpha}(x) dV = w_{q,\alpha}(x_\alpha) = q_\alpha \tag{28}$$

If the change of variable (second equation (14)) is applied to (26), we get

$$\begin{aligned} U(w_{q,\alpha}(x)) &= U(q_\alpha + \boldsymbol{\sigma}_{q,\alpha} \cdot (x - x_\alpha)) \\ &= U(q_\alpha) + \frac{\partial U}{\partial q}_{|q=q_\alpha} \boldsymbol{\sigma}_{q,\alpha} \cdot (x - x_\alpha) + 0(x - x_\alpha)^2 \end{aligned} \tag{29}$$

The second order term in (29) is of the same order as the approximation error in (26). We then get a linear reconstruction for u

$$w_{u,\alpha}(x) = u_\alpha + \boldsymbol{\sigma}_{u,\alpha} \cdot (x - x_\alpha) \tag{30}$$

where

$$\boldsymbol{\sigma}_{u,\alpha} = \frac{\partial U}{\partial q}_{|q=q_\alpha} \boldsymbol{\sigma}_{q,\alpha} = (\nabla u)_\alpha + O(h) \tag{31}$$

is a consistent approximation for the gradient of u at cell center. The reconstructions (26) and (30) are distinct but both are second order accurate. The latter is sometimes preferred as it gives better results in many practical cases and we will only use this form in the sequel.

One of the simplest ways to evaluate $\boldsymbol{\sigma}_{u,\alpha}$ is through a least-squares criterion, for instance a best fit between $w_{u,\alpha}$ and the neighboring state variables :

$$\text{Find } \boldsymbol{\sigma}_{u,\alpha} \text{ such as } \quad M_\alpha^j = \sum_{\beta \in v_\alpha^1} (w_{u,\alpha}^j(x_\beta) - u_\beta^j)^2$$

is minimum for every state variable j. (32)

Solving (32) leads to a linear dependency between $\boldsymbol{\sigma}_{u,\alpha}$ and the state variables in V_α^1

$$\boldsymbol{\sigma}_{u,\alpha}^j = \sum_{\beta \in V_\alpha^1} \mathbf{g}_{u,\alpha\beta}(u_\beta^j - u_\alpha^j) \tag{33}$$

Nonlinear limitation can be applied to (33), but direct limitation of interface state variables is generally sufficient (see next section).

Interpolation along interfaces

The preceding reconstruction gives rise to two distinct second order evaluations of u at face center $x_{\alpha\beta}$:

$$\begin{aligned} u_{\alpha\beta} &= w_{u,\alpha}(x_{\alpha\beta}) = u_\alpha + \boldsymbol{\sigma}_{u,\alpha} \cdot a_{\alpha\beta} \\ u_{\beta\alpha} &= w_{u,\beta}(x_{\alpha\beta}) = u_\beta + \boldsymbol{\sigma}_{u,\beta} \cdot a_{\beta\alpha} \end{aligned} \tag{34}$$

In the case of steep variations, some of these state variables can lie far outside the bounds defined by u_α and u_β, and several nonlinear limitation procedures have been implemented to replace $u_{\alpha\beta}$ and $u_{\beta\alpha}$ by

$$u_{\alpha\beta}^{lim} = L(u_{\alpha\beta}, u_\alpha, u_\beta) \quad , \quad u_{\beta\alpha}^{lim} = L(u_{\beta\alpha}, u_\beta, u_\alpha) \tag{35}$$

which lie inside the interval defined by u_α and u_β. The limiting function L is designed to degenerate into classical limiters like Van Leer, Minmod, etc., on Cartesian grids.

The asymmetry between $u_{\alpha\beta}$ and $u_{\beta\alpha}$ (or $u_{\alpha\beta}^{lim}$ and $u_{\beta\alpha}^{lim}$) will be used for upwinding in characteristic fluxes, but other evaluations can be built, for instance arithmetic or Roe mean value

$$u_{\alpha\beta}^{sym} = \frac{1}{2}(u_{\alpha\beta}^{lim} + u_{\beta\alpha}^{lim}) \quad , \quad u_{\alpha\beta}^{roe} = U^{roe}(u_{\alpha\beta}^{lim}, u_{\beta\alpha}^{lim}) \tag{36}$$

An obvious first order approximation of the interface gradient of u is

$$\boldsymbol{\sigma}'_{u,\alpha\beta} = \frac{|\mathbf{b}_{\beta\alpha}|}{|\mathbf{h}_{\alpha\beta}|}\boldsymbol{\sigma}_{u,\alpha} + \frac{|\mathbf{b}_{\alpha\beta}|}{|\mathbf{h}_{\alpha\beta}|}\boldsymbol{\sigma}_{u,\beta} \tag{37}$$

but a compact evaluation of the normal gradient is also available from u_α , u_β ,

$$\boldsymbol{\sigma}''_{u,\alpha\beta} = \frac{u_\beta - u_\alpha}{\mathbf{n}_{\alpha\beta} \cdot \mathbf{h}_{\alpha\beta}}. \tag{38}$$

It is possible to combine these two evaluations for a consistent one-parameter family of interface gradients

$$\boldsymbol{\sigma}_{u,\alpha\beta} = \boldsymbol{\sigma}'_{u,\alpha\beta} + \theta(\boldsymbol{\sigma}''_{u,\alpha\beta} - \boldsymbol{\sigma}'_{u,\alpha\beta} \cdot \mathbf{n}_{\alpha\beta})\mathbf{n}_{\alpha\beta} \tag{39}$$

If $\theta = 1$, (37) is used only for the non-normal contribution of the gradient, whereas the normal part stems from the compact evaluation (38). This evaluation of gradient has been studied in [27] and proved very effective for dissipative fluxes.

Discrete conservation laws

As indicated before, each surface or volume integral at the right-hand side of (22) needs only one quadrature point:

$$\frac{d}{dt}(V_\alpha q_\alpha) = -\sum_{\beta \in V_\alpha^1} \left[\; q(v - v_A) + \mathbf{f} + \varphi \; \right]_{\alpha\beta} \cdot \mathbf{N}_{\alpha\beta} + V_\alpha \left[\; s \; \right]_\alpha \tag{40}$$

where the subscripts $\alpha\beta$ and α stand respectively for the center of face $x_{\alpha\beta}$ and cell x_α .
Setting

$$F_n \triangleq (q(v - v_A) + \mathbf{f}) \cdot \mathbf{n}, \quad \text{and} \quad \varphi_n \triangleq \varphi \cdot \mathbf{n} \tag{41}$$

(40) reads more simply

$$\frac{d}{dt}(V_\alpha q_\alpha) = -\sum_{\beta \in V_\alpha^1} \left[\; F_n + \varphi_n \; \right]_{\alpha\beta} |\mathbf{N}_{\alpha\beta}| + V_\alpha \left[\; s \; \right]_\alpha \tag{42}$$

Numerical fluxes

The last step will be to pinpoint the numerical fluxes used on the right-hand side of (42):

- The non-dissipative flux density $\left[\; F_n \; \right]_{\alpha\beta}$ from T_α to T_β is evaluated through an approximate Riemann solver using $u_{\alpha\beta}^{lim}$ and $u_{\beta\alpha}^{lim}$ as arguments. Among many other possibilities, we can cite the Roe numerical flux:

$$\begin{aligned} \left[F_n\right]_{\alpha\beta} &= \frac{1}{2}(F_n(u_{\alpha\beta}^{lim}) + F_n(u_{\beta\alpha}^{lim})) \\ &\quad + \frac{1}{2}\left|\frac{\partial F_n}{\partial q}\right|_{\alpha\beta}^{roe} (Q(u_{\alpha\beta}^{lim}) - Q(u_{\beta\alpha}^{lim})) \end{aligned} \tag{43}$$

where the Jacobian matrix $\frac{\partial F_n}{\partial q}$ is evaluated for the Roe mean value of $u_{\alpha\beta}^{roe}$.

- The dissipative flux is evaluated directly from the constitutive law for ϕ

$$\left[\varphi_n\right]_{\alpha\beta} |\mathbf{N}_{\alpha\beta}| = \varphi(u_{\alpha\beta}^{sym}, \boldsymbol{\sigma}_{u,\alpha\beta}) \cdot \mathbf{N}_{\alpha\beta} \tag{44}$$

Properties

These methods have been used for several years in the Eulerian solvers of CEDRE (multispecies fluid flow, Eulerian model for dispersed particles, heat conduction in solids, see examples of calculation results in [37]). Feedback from numerous calculations as well as theoretical studies [17] shows that:

- The above procedure usually gives stable calculations provided that mesh resolution is adequate and the numerical fluxes are adapted to the physics. However, instability can occur when the information from neighborhood V_1 is not sufficient for gradient calculation in some directions: this occurs almost inexorably on tetrahedral meshes in three dimensions. This problem has been thoroughly studied in [16] [17], which shows that using the second neighborhood V_2 is mandatory in that case ; this work provides simple ways to define second neighborhood stable interpolations based on post-processing of (31). Among many other important results, this thesis also shows that the mean-square method tends to be optimal for stability.
- For unsteady simulations, the predominant error in the sense of the modified (equivalent) equation is second order dispersive, which may be insufficient for Large Eddy Simulation or acoustics.

Methods for higher order reconstruction ($k>1$)

In theory, k -exact polynomial reconstructions lead to finite volume discretizations of order $k+1$. The case $k=3$ is of particular importance because 4-th order discretizations dramatically reduce the numerical dissipation, which makes them very valuable for applications in Large Eddy Simulation (LES) and acoustics. In the practice of computations on unstructured grids, however, there are several obstacles to this approach.

- First, the stencil size for k -exact reconstruction of polynomials in d dimensions must be at least equal to $\binom{d+k}{k}$. Recent work [16] [18] has shown that the stability of the MUSCL scheme requires stencil sizes that are several times larger than this minimal size. On unstructured grids, the connectivity data, i.e. which cells contribute to the reconstruction in a specific cell, must be computed, sorted and accessed during runtime.
- Second, a modern unstructured CFD code like CEDRE runs on parallel architectures with a large number of processors, each of which handles a small domain of the partitioned grid. Cells near a domain border may have a reconstruction stencil that overlaps the other domain. For those cells, the connectivity data must be handled and transferred from domain to domain. Furthermore, the size of the overlapping parts of the stencils may vary from cell to cell, creating the need to send data packets of varying length from processor to processor. This can seriously impair the scalability of the code, i.e. the capability to run n times faster on a system with n times the number of processors.

These problems suggest the need for k -exact reconstruction algorithms that require only data exchange between adjacent cells. This can be done in the following way: A polynomial p of degree k is completely determined by its cell average over T_α and its k derivatives at the barycenter of the cell. A k -exact reconstruction is therefore equivalent to the exact reconstruction of the m -th derivatives for $1 \le m \le k$. In practice, such a reconstruction of the m -th derivative will be a sum of the form

$$w_\alpha^{(m)} = \sum_{\beta \in \mathsf{W}_\alpha} w_{\alpha\beta}^{(m)} u_\beta \tag{45}$$

where W_α is a reconstruction stencil that may be very large. For k -exactness one must have

$$w_\alpha^{(m)} = \sum_{\beta \in \mathsf{W}_\alpha} w_{\alpha\beta}^{(m)} u_\beta = D^{(m)} u\Big|_{\mathbf{x}_\alpha} \tag{46}$$

whenever u is a polynomial of degree k . The main idea is to replace the sum over the large neighborhood W_α in (45) by a successive sum over the first neighborhood V_1

$$w_\alpha^{(m)} = \sum_{\beta \in V_1} \tilde{w}_{\alpha\beta}^{(m)} \cdot \sum_{\gamma \in V_1} w_{\beta\gamma}^{(m)} u_\gamma \tag{47}$$

This approximation method can be seen as analogous to exact differentiation where the m -th derivative is obtained by successive differentiation, i.e. $D^{(m)}u = D^{(1)} \cdot D^{(m-1)}u$ The principal challenge is of course to preserve the k -exactness of the reconstruction in (37). Such methods have recently been developed at the DSNA department of Onera for $k=2$ and $k=3$. They have been successfully tested for the linear advection equation. Figure 17 shows the result of the linear advection of a Gaussian hat in 2D.

Last but not least, the use of k -exact polynomial reconstruction requires the use of higher order quadratures to compute the numerical fluxes at the cell interfaces with the necessary precision, otherwise the order of the numerical scheme will be reduced. Quadratures that are exact on polynomials of degree $k=3$ are already implemented in CEDRE ■

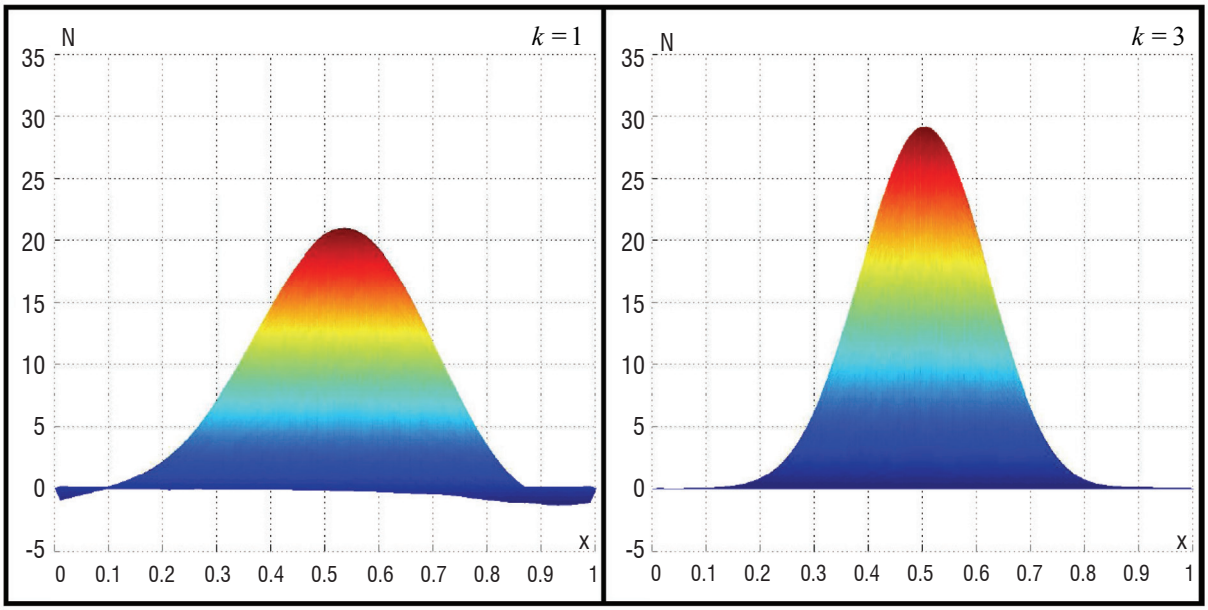

Figure 17 - Advection of a Gaussian hat with $k=1$ and $k=3$

References

[1] B. AUPOIX, F. CHEDEVERGNE, D. ARNAL, E. LAROCHE, S. DECK and F. GLEIZE - *Transition and Turbulence Modelling* . Aerospace Lab. Issue 2. 2011.

[2] C. BENOIT and G. JEANFAIVRE - *Three Dimensional Inviscid Isolated Rotor Calculations Using Chimera and Automatic Cartesian Partitioning Methods.* Journal of the American Helicopter Society, (2003), pp. 128-138.

[3] G. BILLET and J. RYAN - *A Runge Kutta Discontinuous Galerkin Approach to Solve Reactive Flows: the Hyperbolic Operator.* submitted to Journal of Computational Physics.

[4] P. CALI, V. COUAILLIER and A. JAMESON - *Conservative Interfacing for Turbomachinery Applications*. ASME Paper 2001-GT-357, 2001.

[5] W.J. CALVERT, A.W. STAPLETON, P.R. EMMERSON, C.R. BUCHANAM and C.M. NOTT - *Evaluation of a 3D Viscous Code for Turbomachinery*. ASME paper 97-GT-78, 1997.

[6] L. CAMBIER - *ElsA Software.* Aerospace Lab. Issue 2. 2011.

[7] L. CAMBIER and M. GAZAIX - *elsA – An Efficient Object Oriented Solution to CFD Complexity.* AIAA Paper 2002-0108, 2002.

[8] R.V. CHIMA - *Viscous Three-Dimensional Calculations of Transonic Fan Performance.* AGARD CP 510, Paper 21, 1991.

[9] P. CINNELLA and A. LERAT - *A Study of Turbulent Compressible Flows Over Oscillating Airfoils Using a High-Order Numerical Scheme.* Computational Fluid Dynamics Journal special issue, 9 (2001), pp. 257-271.

[10] V. COUAILLIER, P. VEYSSEYRE and A.M. VUILLOT - *3-D Navier-Stokes Computations in Transonic Compressor Bladings*. Proceedings of the 10th ISABE Conference, 1991.

[11] R.L. DAVIS, R.H. NI and J.E. CARTER - *Cascade Viscous Flow Analysis Using the Navier-Stokes Equations.* Jour. Of Propulsion, Vol. 3, pp 406-414, 1987

[12] F. DUPOIRIEUX, N. BERTIER, V. SABELNIKOV and P. GILBANK - *The Models of Turbulent Combustion in the CHARME Solver of CEDRE* . Aerospace Lab. Issue 2. 2011.

[13] D. DUTOYA and L. MATUSZESKI - *Thermodynamics in CEDRE* . Aerospace Lab. Issue 2. 2011.

[14] C.A.J. Fletcher - *Computational Techniques for Fluid Dynamics Specific Techniques for Different Flow Categories*, 2nd edition, Springer, 1991.

[15] M.B. GILES - *Stator/Rotor Interaction in a Transonic Turbine*. AIAA Paper 88-3093.

[16] F. HAIDER - *Discrétisation en maillage non structuré général et application.* Phd Thesis, Université Pierre et Marie Curie, 2009

[17] F. HAIDER, J.P. CROISILLE and B. COURBET - *Stability of the Muscl Method on General Unstructured Grids for Applications to Compressible Flows*, Fifth International Conference on Computational Fluid Dynamics, Seoul, 2008 Springer Verlag

[18] F. HAIDER, J.P. CROISILLE and B. COURBET - *Stability Analysis of the Cell Centered Finite-Volume Muscl Method on Unstructured Grids Numer.* Math., vol. 113, 2009, pp. 555-600

[19] C. HIRSCH - *Numerical Computation of Internal and External Flows*. John Wiley & Sons, 1988

[20] C. HIRSCH - *Numerical Computation of Internal and External Flow*. Fundamentals of Computational Fluid Dynamics, Butterworth-Heinemann Elsevier, Second edition 2007

[21] A. JAMESON, W. SCHMIDT, and E. TURKEL - *Numerical Solutions of the Euler Equations by Finite Volume Methods Using Runge-Kutta Time Stepping,* AIAA Paper, 81-1259 (1981).

[22] N. KROLL - MEGAFLOW – *A Numerical Flow Simulation System*. Proceedings of the ICAS Conference, Melbourne, 1998.

[23] M. LEFÈBVRE - *Développement de nouvelles techniques numériques pour la resolution des equations de Navier-Stokes tridimensionnellles stationnaires sur des maillages hybrides structurés/non structurés.* Thèse de doctorat « thermique et énergétique », Ecole Centrale de Lyon, 1998.

[24] M. LEFÈBVRE, V. COUAILLIER and J.M. DUBOUÉ - *Numerical Methods on Adaptative Hybrid Grids for the Solution of Euler and Navier-Stokes Equations.* Proceedings of the 4th ECCOMAS Conference, J. Wiley, 1998.

[25] J.-M. LE GOUEZ, V. COUAILLIER and F. RENAC - *High Order Interpolation Methods and Related Urans Schemes on Composite Grids*. 48th AIAA Aerospace Sciences Meeting, Orlando, Florida, 2010

[26] A. LERAT - *Implicit Methods of Second-Order Accuracy for the Euler Equations.* AIAA Computational Fluid Dynamics Conference, Danvers, 1983.

[27] N. LETERRIER - Discrétisation spatiale en maillage non-structuré de type général. Phd Thesis, Université Pierre et Marie Curie, 2003

[28] C. MARMIGNON, V. COUAILLIER and B. COURBET - *Solution Strategies for Integration of Semi-Discretized Flow Equations in elsA and CEDRE*. Aerospace Lab. Issue 2. 2011.

[29] R. MEAKIN - *Adaptive Spatial Partitioning and Refinement for Overset Structured Grids*. Computer Methods in Applied Mechanics and Engineering, 189 (2000), pp. 1077- 1117.

[30] A. MURRONE and P. VILLEDIEU - *Numerical Modelling of Dispersed Two-Phase Flow* . Aerospace Lab. Issue 2. 2011

[31] R.H. NI - *A Multiple Grid Scheme for Solving the Euler Equations.* AIAA Journal, Vol. 20, pp. 1565-1571, 1982.

[32] R. PEYRET and T.D. TAYLOR - *Computational Methods for Fluid Flow*. Springer Verlag, 1983.

[33] A. Refloch, et Al. - *CEDRE Software*. Aerospace Lab. Issue 2. 2011

[34] J. RENEAUX and al - *Advanced Aerodynamic Applications with the elsA Software*. Aerospace Lab. Issue 2. 2011

[35] A. REZGUI, P. CINNELLA, and A. LERAT - *Third-Order Accurate Finite Volume Schemes for Euler Computations on Curvilinear Meshes*. Computers and Fluids, 30 (2001), pp. 875-901.

[36] O. SAUNIER, C. BENOIT, G. JEANFAIVRE, and A. LERAT - *Third-Order Cartesian Overset Mesh Adaptation Method forSolving Steady Compressible Flow*. International Journal for numerical methods in fluid, 57 (2008), pp. 811-838.

[37] D. SCHERRER and al - *Recent CEDRE Applications*. Aerospace Lab. Issue 2. 2011

[38] J. STEGER, F. DOUGHERTY, and J. BENEK - *A chimera grid scheme.* Advances in Grid Generation. K.N. Ghia and U. Chia, eds., ASME FED, 5 (1983), pp. 59-69.

[39] B. VAN LEER - *Towards the Ultimate Conservative Difference Scheme V. A Second-Order Sequel to Godunov's Method.* Journal of Computational Physics, vol. 32, no 1, pp, 101-136, 1979

[40] A.M. VUILLOT, V. COUAILLIER and N. LIAMIS - *3D Turbomachinery Euler and Navier-Stokes Calculations with a Multi-Domain Cell-Centered Approach.* AIAA paper 93-2576, 1993.

[41] A. WISSINK, M. POTSDAM, and V. SANKARAN - *A Coupled Unstructured-Adaptive Cartesian CFD Approach for Hover Prediction.* 66th AHS Forum, 2010.

AUTHORS

Bernard Courbet Ecole Centrale Paris, Research engineer, department of numerical simulation and aeroacoustics, unit CIME Architect and developer for the CEDRE software, numerical methods for polyedral meshes.

Christophe Benoit Ecole Centrale Nantes, Doctoral Degree, Mechanics, ENSAM Research engineer, department of numerical simulation and aeroacoustics, unit CS2A Numerical geometry and mesh.

Vincent Couaillier Doctoral degree Master in Numerical Analysis University Pierre et Marie Curie (UPMC) Head of the unit NUMF (Numerical Methods for Fluid Mechanics), department of numerical simulation and aeroacoustics Algorithms and software developments.

Florian Haider Master of Physics, University of Technology, Vienna Austria Master of Mathematics (Analysis and Geometry), University Pierre et Marie Curie Paris 6 Master of Mathematics (Mathematics and Applications), University Pierre et Marie Curie Paris 6 Doctoral Degree, Mechanics, University Pierre et Marie Curie Paris 6 Research engineer, department of numerical simulation and aeroacoustics, unit CIME Research on numerical methods for unstructured grids, software development for the project CEDRE

Marie-Claire Le Pape Ecole Centrale Lyon, Research engineer, department of numerical simulation and aeroacoustics, unit NUMF Chimera methods, hybrid mesh development and validation in ELSA

Stéphanie Péron Ecole Centrale Marseille DEA ENS Cachan Research engineer, department of numerical simulation and aeroacoustics, unit CS2A Mesh generation, adaptation and assembling, Cartesian solver with third order schemes.